Scaling law for growth of misoriented equiaxed Al-Cu dendrites: A phase-field study with in situ experiment validation

Tongzhao Gong, Yun Chen, Xing-Qiu Chen, Dianzhong Li, Guillaume Reinhart, Henri Nguyen-Thi, Jean-Marc Debierre

Scaling law for growth of misoriented equiaxed Al-Cu dendrites: A phase-field study with in situ experiment validation

Gong, TZ (Gong, Tongzhao) [1] ; Chen, Y (Chen, Yun) [1] ; Chen, XQ (Chen, Xing-Qiu) [1] ; Li, DZ (Li, Dianzhong) [1] ; Reinhart, G (Reinhart, Guillaume) [2] ; Nguyen-Thi, H (Nguyen-Thi, Henri) [2] ; Debierre, JM (Debierre, Jean -Marc) [2]

[1] Inst Met Sci & Technol, Chinese Acad Sci, Shenyang Natl Lab Mat Sci, Shenyang, Peoples R China
[2] Aix Marseille Univ, Univ Toulon, CNRS, IM2NP UMR 7334, F-13397 Marseille, France

Abstract

We consider the effect of a mutual misorientation between two interacting equiaxed dendrites in polycrystalline materials on the scaling law of growth from undercooled melt. This effect is investigated by three-dimensional quantitative phase-field simulations of Al-Cu alloy solidification in thin samples. It has been found that the equiaxed dendritic growth kinetics changes due to the reduced solute interaction when considering mutual grain misorientation, and both the characteristic growth rate and primary dendritic arm length can be approximately correlated linearly to the misorientation of two dendrites. The scaling law, which originally uses the solute composition and the distance between two nuclei as physical parameters to describe the dynamics of primary dendritic arms, is then adapted with consideration of the misorientation. Compared with the previous scaling law that only concerns face-to-face growth of two dendrites, the predictions of the newly proposed scaling law taking the grain orientation in account are in better agreement with the experimental data.

Keywords : Solidification, Equiaxed dendrite, Al-Cu alloys, Growth dynamics, Phase-field method

1. Introduction

Microstructure formed during solidification strongly determines performance of materials, such as mechanical properties and corrosion resistance [1], [2]. The dendrite is one of the most common solidification microstructures, and the equiaxed grain is usually preferred in practice to columnar grain, in order to obtain homogeneous and isotropic mechanical

properties in industrial metallic manufacture like aeronautics and automotive. Over the last few decades, many experimental studies have focused on the equiaxed solidification process, and it has been revealed that two growth kinetic stages are successively experienced by the equiaxed grain after nucleation, namely the free growth and impinged growth regimes [3], [4]. At the beginning of the equiaxed grain growth in the early stages of solidification, a dendritic grain is isolated from its neighbors, thus leading to an ever-increasing growth rate with increasing undercooling. Whereafter, due to the solute rejection into liquid around the dendrite during the liquid to solid transformation, a solute diffusion layer progressively builds up ahead of the solid–liquid interface. After a while, the solute layer overlaps with that of neighboring grains, which makes the dendrite growth slow down and even almost stop when the solute interaction between neighboring grains becomes strong enough. These two processes are responsible for the formation and evolution of the grain structure in most polycrystalline materials.

In addition to experimental studies, several numerical methods have been proposed to investigate the equiaxed dendrite growth during alloy solidification, as well as the underlying physical mechanisms [1], [2]. The quantitative phase-field (PF) approach, based on the thin-interface limit [5] and solute anti-trapping current [6], [7], has been recognized as the most powerful tool to simulate dendrite growth because it avoids the explicit tracking of the complicated solid–liquid interface [8], [9], [10]. Moreover, large-scale quantitative PF simulations have been realized by means of the increasingly developed advanced numerical algorithms, such as adaptive mesh refinement/coarsening and GPU parallel computing, which also provides convenient tools to study solidification [11], [12], [13], [14]. Using the quantitative PF method combined with in situ and real-time observation of solidification experiments by synchrotron X-ray radiography, many works have been carried out to investigate the growth and interaction of equiaxed dendrite during solidification [15], [16], [17], [18], and a scaling law has been proposed to describe the dynamics of dendritic primary arms, with the solute composition and the average distance between two nuclei as physical parameters, which is given as [16], [17]

$$\frac{L_{\mathrm{m}}}{L} = \Lambda \tag{1}$$

where the characteristic primary dendritic arm length is $L_{\mathrm{m}} = V_{\mathrm{m}}\Delta t_{\mathrm{m}}$, V_{m} is the maximum growth rate of the primary arm tip, $\Delta t_{\mathrm{m}} = t_{\mathrm{m}} - t_{\mathrm{m}}'$ with t_{m} and t_{m}' respectively corresponding to V_{m} and $V_{\mathrm{m}}' = V_{\mathrm{m}} / 2$, $2L$ is the initial distance between two nuclei, and Λ is a constant which is

independent of the alloy composition. It has been indicated that $\Lambda = 0.537$ is a reasonable value for equiaxed Al-Cu dendrites in thin samples, which has been validated by in situ and real-time observed solidification experiments [16] and then revised by incorporating thermodynamic effects [17]. However, the scaling law proposed in these two studies [16], [17] only focused on the simple ideal case, in which the primary dendrite arms of two grains grew in exactly opposite directions. However, the grain orientation in most of polycrystalline materials is random. Therefore, one can suspect that the value of constant Λ and the scaling law should also be related to the misorientation between primary dendrite arms of two neighboring grains.

In this paper, the effect of misorientation between two grain primary arms on the scaling law (1) is studied by using quantitative 3D PF simulations, accelerated by the fast simulation schemes proposed in our previous work [14], including the nonlinear preconditioning of the diffusive interface model, the front-tracking method to capture the orientation of grains, and the parallel adaptive finite element method. The growth kinetics of the primary arm of an equiaxed dendrite is quantitatively discussed. A novel scaling law that takes the crystallographic orientation into consideration is proposed and then validated via the in situ and real-time observation of solidification of Al-Cu alloys by synchrotron X-ray radiography.

2. Model description and numerical implementations

2.1. Phase-field model

The quantitative PF model presented in Ref. [7] is adopted to simulate isothermal solidification of binary alloys under the continuous cooling condition. The quantitative capability of this model to reproduce time evolution of microstructure during alloy solidification has been demonstrated in many previous studies [16], [19], [20], [21]. The governing equations of the phase field ϕ and the rescaled solute concentration U are respectively given as

$$\left(1+\frac{R_c t}{|m|C_0}\right)\tau(\boldsymbol{n})\frac{\partial\phi}{\partial t}=\nabla\cdot\left[W(\boldsymbol{n})^2\nabla\phi\right]+\sum_{i=x,y,z}\partial_i\left[|\nabla\phi|^2 W(\boldsymbol{n})\frac{\partial W(\boldsymbol{n})}{\partial(\partial_i\phi)}\right] \quad (2)$$
$$+\phi-\phi^3-\lambda\left[U-\frac{R_c t}{(1-k)|m|C_0}\right]\left(1-\phi^2\right)^2$$

$$\frac{(1+k)-(1-k)\phi}{2}\frac{\partial U}{\partial t}=\nabla\cdot\left\{D\frac{1-\phi}{2}\nabla U+\frac{W_0[1+(1-k)U]}{2\sqrt{2}}\frac{\partial\phi}{\partial t}\frac{\nabla\phi}{|\nabla\phi|}\right\} \quad (3)$$
$$+\frac{1+(1-k)U}{2}\frac{\partial\phi}{\partial t}$$

with

$$U=\frac{2C/C_0-[(1+k)-(1-k)\phi]}{(1-k)[(1+k)-(1-k)\phi]} \quad (4)$$

where C is the local solute concentration, C_0 is the initial concentration, k is the solute partition coefficient, R_c is the cooling rate, and m is the liquidus slope. The solid and liquid phases are represented by $\phi = +1$ and $\phi = -1$, respectively.

The spatial length and time are rescaled respectively by the interface width W_0 and relaxation time τ_0, and therefore the dimensionless value for the solute diffusion coefficient in liquid is

$$\widetilde{D}=\frac{D\tau_0}{W_0^2}=a_1 a_2\frac{W_0}{d_0} \quad (5)$$

where $d_0 = \Gamma/[mC_0(k-1)]$ is the chemical capillary length with Γ the Gibbs-Thomson coefficient, $a_1 =$ and $a_2 = 47/75$ [7]. The coupling coefficient λ in Eq. (2) is taken as $\lambda = a_1 W_0/d_0$. The standard form of the fourfold symmetry of the surface energy anisotropy is considered, and thus $W(\mathbf{n}) = W_0 a_s(\mathbf{n})$ and $\tau(\mathbf{n}) = \tau_0 a_s(\mathbf{n})^2$ where

$$a_s(\boldsymbol{n})=1-3\varepsilon_4+4\varepsilon_4\sum_{i=x,y,z}\frac{(\partial_i\phi)^4}{|\nabla\phi|^4} \quad (6)$$

In order to accelerate large-scale quantitative PF simulations, a nonlinear preconditioning [22] of the phase field ϕ is employed to allow coarser grids to be used in the interface layer. The transformed phase field ψ is given as

$$\psi=\tanh\left(\frac{\phi}{\sqrt{2}}\right) \quad (7)$$

And hence the standard PF model (Eqs. (2), (3)) is transformed to the nonlinear preconditioned formula, as follows:

$$\left(1+\frac{R_c t}{|m|C_0}\right)\tau_0 a_s^2(\boldsymbol{n})\frac{\partial\psi}{\partial t} = W_0^2 a_s^2(\boldsymbol{n})\left[\nabla^2\psi - \sqrt{2}\tanh\left(\frac{\psi}{\sqrt{2}}\right)|\nabla\psi|^2\right] \quad (8)$$
$$+\sum_{i=x,y,z} W_0^2\partial_i\left[|\nabla\psi|^2 a_s(\boldsymbol{n})\frac{\partial a_s(\boldsymbol{n})}{\partial(\partial_i\psi)}\right]+\sqrt{2}\tanh\left(\frac{\psi}{\sqrt{2}}\right)$$
$$-\sqrt{2}\lambda\left[1-\tanh^2\left(\frac{\psi}{\sqrt{2}}\right)\right]\left[U-\frac{R_c t}{(1-k)|m|C_0}\right]$$

$$\frac{(1+k)-(1-k)\tanh\left(\frac{\psi}{\sqrt{2}}\right)}{2}\frac{\partial U}{\partial t} \quad (9)$$
$$=\nabla\cdot\left\{D\frac{1-\tanh\left(\frac{\psi}{\sqrt{2}}\right)}{2}\nabla U+\frac{1}{2}W_0[1+(1-k)U]\frac{1-\tanh^2\left(\frac{\psi}{\sqrt{2}}\right)}{2}\frac{\partial\psi}{\partial t}\frac{\nabla\psi}{|\nabla\psi|}\right\}$$
$$+\frac{1+(1-k)U}{2}\frac{1-\tanh^2\left(\frac{\psi}{\sqrt{2}}\right)}{\sqrt{2}}\frac{\partial\psi}{\partial t}.$$

The numerical accuracy and efficiency of the preconditioned PF formula has been examined and validated [14]. The detailed numerical and material parameters can be referred to our previous studies [15], but here C_0 is set to be 1 wt% to result in a larger capillary length. Large-scale simulations can be therefore realized quantitatively in a relatively wide range of grain misorientation. In addition, for consistency of conclusions, the values of several material parameters, such as the solute diffusion coefficient in liquid, the slope of liquidus, the anisotropy strength of interfacial energy and the Gibbs-Thomson coefficient are the same as those in the recent literature [16], [17].

2.2. Convergence test

To achieve quantitative 3D PF simulations, the interface width, W_0, must be carefully determined to obtain a reasonable compromise between the computational accuracy and efficiency. The numerical convergence test is carried out for the simulation with $\Delta\theta = 2\alpha = 90°$ and the distance between two nuclei is $2L = 1600$ μm, for which the dendrites grow in the fastest rate. $\Delta\theta$ is the angle between the direction of primary dendrite arm growth of two grains in the thin sample, and α is the misorientation. The two grains are placed in the same *xOy* plane, so that the misorientation is preset by rotating the dendrites around the *z*-axis, and the specific configuration of two mutually misoriented interacting dendrites can be seen in Fig. 1. It is assumed that both grains nucleate simultaneously and therefore the grain morphologies are the same.

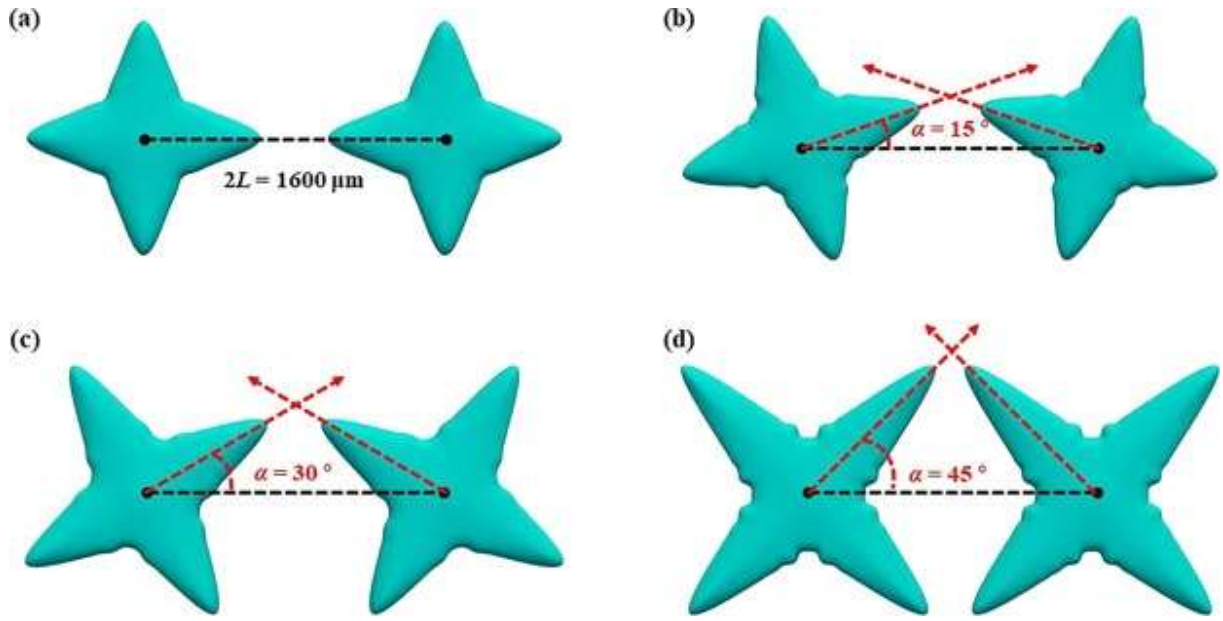

Fig. 1. Configuration and morphology of the two interacting equiaxed Al-1.0 wt% Cu dendrites at t_m *with different misorientations and* L *= 800 μm. (**a**)* α *= 0; (**b**)* α *= 15°; (**c**)* α *= 30°; (**d**)* α *= 45°. The red dashed arrows represent the growth directions of primary arm tips. (For interpretation of the references to colour in this figure legend, the reader is referred to the web version of this article.)*

The simulated tip velocities of the primary dendrite arm with different interface width in the numerical convergence test are plotted in Fig. 2. As expected, a good convergence is observed as W_0 is reduced. However, the computing amount will also increase significantly with W_0 decreasing, which means that we need to enlarge W_0 to reach accessible computing time. The maximum tip velocities at the end of the free growth stage, V_m, are 30.2, 34.3 and 35.4 μm/s, respectively for the cases with W_0 = 2.5, 2.0 and 1.6 μm. The relative deviation of V_m for the cases with W_0 = 2.0 and 1.6 μm is only about 3 %, so it is reasonable to make a choice of W_0 = 1.6 μm for all the 3D PF simulations in the present work.

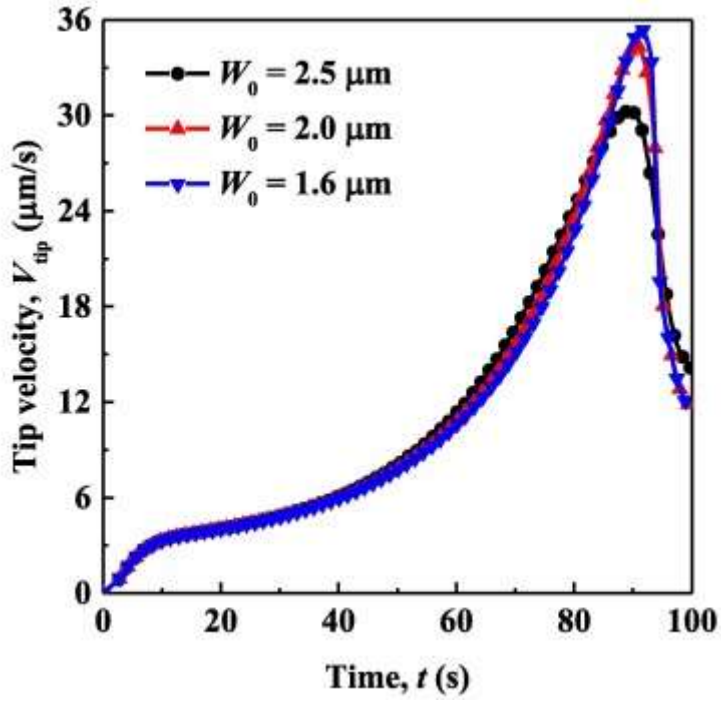

*Fig. 2. Tip velocities of the equiaxed Al-1.0 wt% Cu dendrites with α = 45° and the initial distance between two nuclei being 2*L *= 1600 μm.*

2.3. Numerical implementations

The parallel adaptive finite element method, with multiple processors using distributed memory based on the MPI protocol, is employed to solve the nonlinearly preconditioned PF model. Numerical implementations are realized by the open-source deal.II library [23], and the adaptive mesh refinement/coarsening is achieved through a simple but efficient approach [14]. The front-tracking method [14] is used to capture grain orientations to improve the computing efficiency dramatically. The computational domain size is $4L \times 4L \times 200$ μm (L = 600, 700, and 800 μm), and its thickness is consistent with that of the samples observed in situ and real-time by synchrotron X-ray radiography in the solidification experiments [16]. At the beginning of simulations, the center-to-center distance between the two nuclei is set to be $2L$ and the two grains nucleate simultaneously with the misorientation being in the range of 0–45°. In simulations, the larger the angle, the larger the maximum growth rate (at the end of the free-growth stage), and consequently the longer the calculation time is. All the simulations were carried out on a supercomputer with an Intel® Xeon E5-2683 v4 CPU (2.10 GHz and 32 cores) and 256 GB memory at each computing node. For the 3D simulation with the largest misorientation (α = 45°) and the largest computational domain size (L = 800 μm), it took about 35 h using 192 cores to finish the computation, when the dendritic growth came into the

impinged-growth regime in which the growth rate of the primary dendrite arm tip sharply decreased.

3. Results and discussions

3.1. Dendrite growth kinetics

The equiaxed dendritic morphologies of two grains with various misorientations at time t_m when the tip growth rate reaches its maximum are shown in Fig. 1. It is visible that the length of the primary dendritic arm increases with increasing the grain misorientation owing to the reduced solute interaction. The reason for the reduced solute interaction can be attributed to the fact that the solute boundary layer overlapping is delayed when misorientation is larger. Therefore, it seems natural to conclude that there are significant differences in dendrite growth kinetics with various misorientations, resulting in that the effect of the dendrite orientation must be considered in the scaling law (1) to give a more general description of equiaxed dendrite growth in polycrystalline materials.

In order to compare the dendrite growth kinetics in detail, the growth velocities of the primary dendrite arm tips (marked by the red arrows as shown in Fig. 1) are measured, and the results are plotted in Fig. 3. Without misorientation ($\alpha = 0$), the maximum tip growth velocity $V_{m,0}$ as well as the characteristic length of the primary dendrite arm $L_{m,0}$ are both given in Table 1. The results of the present work are in quite good agreement with the reference values [16], [17]. The relative error due to the measurement time interval or calculation method is less than 10 %, both in terms of the tip growth velocity and the characteristic primary arm length. And this also adequately confirms that the simulated results in the present work are sufficiently reliable to study the effect of mutual misorientation of two interacting equiaxed dendrites on the scaling law.

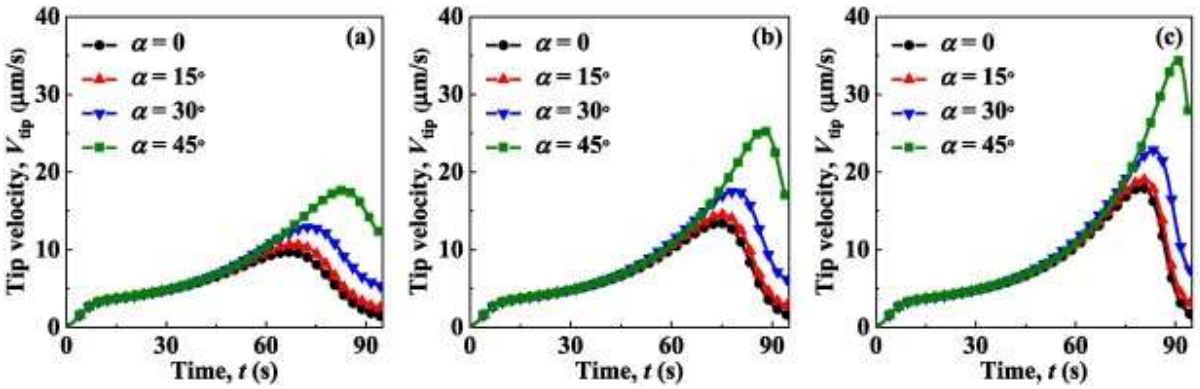

*Fig. 3. Growth kinetics of the equiaxed Al-1.0 wt% Cu dendrites for different grain misorientations and computational domain sizes. (**a**)* L *= 600 μm; (**b**)* L *= 700 μm; (**c**)* L *= 800 μm.*

L (μm)	$V_{m,0}$ (μm/s)	Refs. [16], [17]	$L_{m,0}$ (μm)	Refs. [16], [17]
600	9.710	9.360	345.1	322.2
700	13.44	12.74	385.7	375.9
800	18.02	16.64	418.3	429.

Table 1. Comparison of the values of V_m *and* L_m *with* α *= 0 and* L *= 600, 700, and 800 μm, between the present work (*W_0 *= 1.6 μm) and prediction by scaling laws in references [16], [17].*

Moreover, as can be seen in Fig. 3, the tip growth velocity at the same time (or undercooling) increases gradually with misorientation, which is due to the decreasing solute interaction between neighboring grains. To be specific, the ratio between the maximum tip velocity and the value with $\alpha = 0$ could be expressed as a power function of the misorientation, namely

$$\frac{V_m}{V_{m,0}} = 1 + a\alpha^b \tag{10}$$

with a and b being two positive fitting parameters. The values of $V_m/V_{m,0}$ are shown in Fig. 4**(a)**, from which it is obvious that $V_m/V_{m,0}$ evolves with α as a power function. The power correlation with the misorientation is also valid for the ratio of the characteristic primary arm length, $L_m/L_{m,0}$, which could be written as

$$\frac{L_m}{L_{m,0}} = 1 + a'\alpha^{b'} \quad (11)$$

with *a*' and *b*' being two other positive fitting parameters. The power relationship between the characteristic primary arm length and misorientation could be confirmed further from Fig. 4**(b)**. In general, a clear conclusion which can be drawn from Fig. 4 is that, the solute interaction between the primary dendrite arm of two neighboring grains will be changed when different grain orientations are taken in account, which leads to the change of dendritic growth kinetics. Consequently, the scaling law proposed for $\alpha = 0$ [16], [17] where the grain misorientation was ignored should be necessarily modified to adapt to the present more common situation ($\alpha \neq 0$).

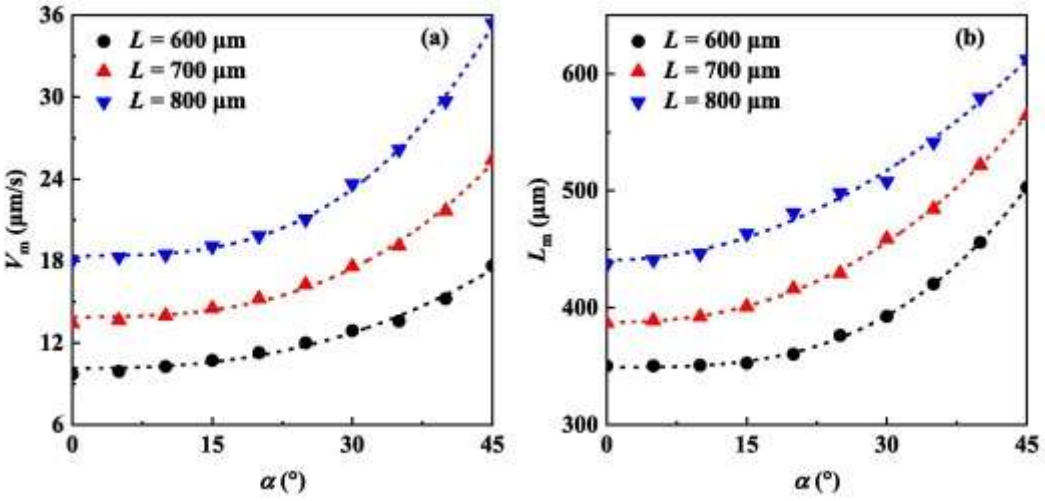

Fig. 4. Plotting of ***(a)*** V_m *and* ***(b)*** L_m *with misorientations* α*. The data points are from the corresponding 3D PF simulations, while the dashed curves are the power law fitting.*

3.2. Scaling law

The previous section reveals that both the maximum tip growth velocity V_m and the characteristic primary arm length L_m are correlated to the misorientation α, as a power function. However, the power relationship is not a general law, since in practice the values of the two fitting parameters in Eq. (10) and Eq. (11) vary with the distance between the two dendrites. What is interesting, though, is that we can find a more general correlation between $V_m/V_{m,0}$ or $L_m/L_{m,0}$ and α. According to Fig. 5**(a)** and Fig. 5**(b)**, there is a quite good linear relationship between $V_m/V_{m,0}$ and $1/\cos^2\alpha$, as well as between $L_m/L_{m,0}$ and $1/\cos\alpha$. Based on

222 this, it is easy to infer that the ratio of $\Delta t_m/\Delta t_{m,0}$ also varies with cosα in an approximate linear
223 manner, which has been validated in Fig. 5**(c)**.

224

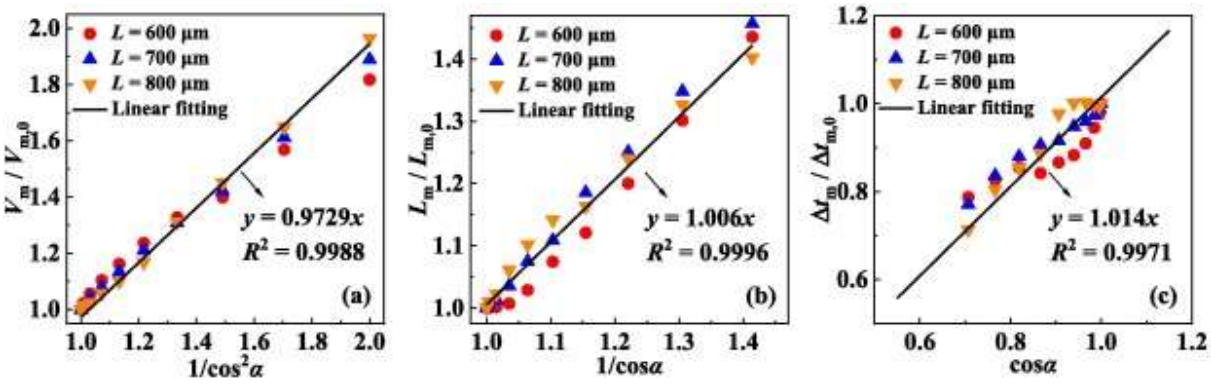

225

226 *Fig. 5. Variation of* ***(a)*** V*m*, ***(b)*** L*m* *and* ***(c)*** *Δ*t*m* *with the grain misorientation* α.

227 For the ratio of $V_m/V_{m,0}$, it could be expressed as $V_m/V_{m,0} = p/\cos^2\alpha$, and the value of the fitting
228 parameter $p \approx 0.9729$ is approximately equal to 1. For the ratio of $L_m/L_{m,0}$, it could be
229 expressed as $L_m/L_{m,0} = q/\cos\alpha$, and the values of the fitting parameter $q \approx 1.006$ is also
230 approximately equal to 1. The rounding of fitting parameters ensures that the values of V_m and
231 L_m exactly reduce to $V_{m,0}$ and $L_{m,0}$ when the misorientation is vanishing ($\alpha = 0$). Therefore,
232 both $V_m/V_{m,0}$ and $L_m/L_{m,0}$ can be written as simple functions of α as

$$\frac{V_m}{V_{m,0}} = \frac{1}{\cos^2\alpha} \tag{12}$$

$$\frac{L_m}{L_{m,0}} = \frac{1}{\cos\alpha} \tag{13}$$

233

234 and then the ratio of $\Delta t_m/\Delta t_{m,0}$ can be derived as

$$\frac{\Delta t_m}{\Delta t_{m,0}} = \cos\alpha \tag{14}$$

235

236 The dynamics scaling considered in the present work focuses on the time interval when the
237 dendrite tip crosses over from a free-growth regime to a poisoned-growth one. Therefore, one
238 can reasonably expect that the scaling in this time interval is not governed by the late solute
239 interaction between dendrites. For the moment, we can thus stick to the assumption that
240 geometric factors are dominant, which is consistent with Eq. (13). Indeed, for $\alpha = 0$ the
241 scaling law $L_m = \Lambda L$ was recently justified on the sole basis of geometric arguments [24]. The
242 Eq. (12) is essentially based on the solute conservation at the interface of the dendritic arm

tip, i. e., $V_i(1-k)C_{L,i} = -D_L|\nabla C_{L,i}|$ where V_i is the propagation of tip interface, $C_{L,i}$ is tip solute concentration, and $|\nabla C_{L,i}|$ is gradient of tip concentration. Moreover, the solute in liquid approximately satisfies the exponential decay function, namely $C(\mathbf{r}) = C_0 + (C_{L,i} - C_0)\exp[-2(\mathbf{r} - \mathbf{r}_0)/L_s]$ with $\mathbf{r}_0$ the position of the tip interface and L_s the width of solute boundary layer. Combining the two relationships above, we can infer that $V_m \propto (1 - C_0/C_{L,i})\cdot(1/L_s)$, and both terms in the product increase as the space of free growth increases. Therefore, it is natural that V_m is proportional to L_m to the second power as $V_m \propto L_m^2 \propto (1/\cos\alpha)^2$.

According to the expressions given in Refs. [16], [17], the final scaling law considering the grain misorientation can be expressed as

$$V_m = V_{m,0}\frac{1}{\cos^2\alpha} \approx 2.6\times 10^{-5}\frac{L^2}{C_0^{2/3}}\frac{1}{\cos^2\alpha} \quad (15)$$

$$L_m = L_{m,0}\frac{1}{\cos\alpha} = \Lambda L\frac{1}{\cos\alpha} \quad (16)$$

where the value of the constant Λ was revealed to be 0.546 for the first time [16], and then re-calibrated to 0.537 through analysis of additional PF simulations considering a curved thermodynamic phase diagram and spatiotemporal noise [17].

3.3. Comparison with experimental data

In order to validate the scaling law considering the grain misorientation, the length of the characteristic primary dendritic arm predictions by Eq. (13) are compared to the experimental data, which was measured from the in situ and real-time observation of the of Al-Cu alloys solidification experiments by synchrotron X-ray radiography [15], [16]. A detailed description of the solidification experiment and in situ and real-time observation is given in [16]. Here we still chose the two dendrites from [16] and one from [15]. For the first dendrite shown in Fig. 6**(a)**, since there is no neighbor grains around the selected arm, the misorientation is measured according to the angle between the selected arm and the horizontal direction, which has a value of α = 9.20°. For the other two dendrites with neighbor grains in Fig. 6(b, c), the misorientations are 9.98° and 51.7°, respectively, which are measured according to Fig. 1.

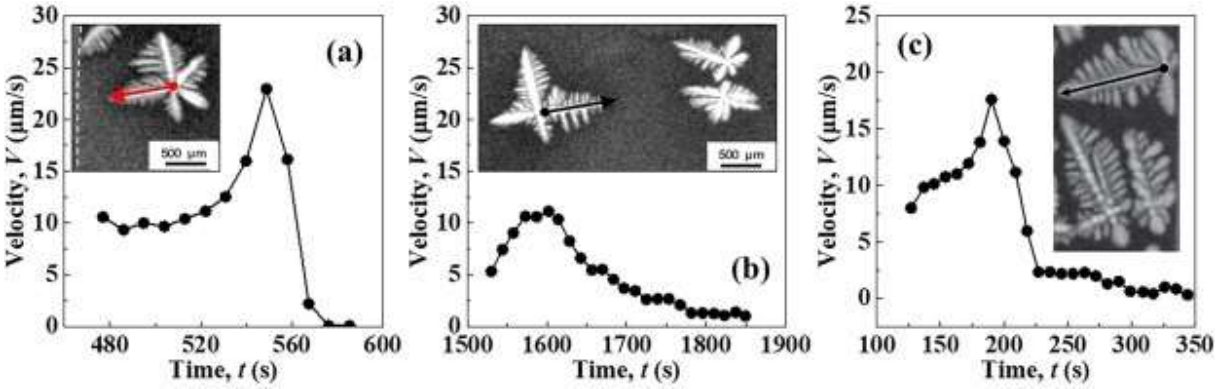

*Fig. 6. Tip growth rates of the three dendrites in the solidification experiments of Al-Cu alloys by isothermal cooling at 0.5 K/min. (**a**) and (**b**) are from [16] and (**c**) is from [15].*

The experimental data and the predictions by the scaling law proposed for $\alpha = 0$ [16], [17] and for $\alpha \neq 0$ (present work) are given in Table 2. The characteristic primary arm length, L_m, is calculated as the product of the maximum tip growth velocity, V_m, and the time interval ($\Delta t_m = t_m - t_m'$) between the time when the tip growth velocity reaches V_m and $V_m / 2$. For the first grain with $\alpha = 9.20°$, the measured characteristic primary length, L_m, is 575 μm. The value predicted for $\alpha = 0$ [16], [17] is 563 μm, while the value predicted for $\alpha = 9.20°$ by Eq. (16) is 571 μm, which is in a better agreement with the experimental data. For the second grain with $\alpha = 9.98°$, the measured characteristic primary length, L_m, is 760 μm, which is quite different from the predicted results of the two scaling laws, regardless of the misorientation is taken into account or not. The reason for this large discrepancy (~15 %) is that the two grains nucleated at different instants, thus leading to that the second grain had already been growing for some time when its neighbors nucleated. As mentioned earlier, in the present PF simulations and the derivation of the scaling law, the difference in nucleation time between neighboring grains is not considered, which could explain why the predicted values are smaller than the experimental data. For the third grain with a larger misorientation ($\alpha = 51.7°$), both lower values predicted by PF simulations compared to experimental data could be attributed to the time lag between grain nucleations. However, the result predicted in this work ($L_m = 805$ μm) is much better than that predicted by the scaling law without misorientation ($L_m = 499$ μm), which suggests that the scaling law considering grain orientation proposed in the present work can indeed predict values more consistent with the experimental data.

		Experimental data		L_m value predicted by Eq. (16)	
L	α	L_m	$\alpha = 0$	$\alpha \neq 0$
μm	degree	μm	μm	μm
1050	9.20	575	563	571
1200	9.98	760	643	654
930	51.7	1036	499	805

Table 2. Comparison of the values of the characteristic primary arm length between the experiment and predictions by scaling laws.

4. Conclusions and outlooks

In the present work, the effect of the grain orientation on the scaling law of equiaxed dendrite growth of Al-Cu alloys [16], [17] was investigated by quantitative 3D PF simulations. It was revealed that for random grain orientations, which is the case in polycrystalline materials, the solute interaction between two neighboring grains was generally reduced and the grain growth kinetics changed accordingly. To be more specific, the duration of the free-growth period of the equiaxed dendritic growth was shown to be longer with the increase of the misorientation, so that the maximum dendritic tip growth rate V_m and the characteristic primary dendritic arm length L_m also increase. Therefore, a good correlation of V_m or L_m with grain misorientation was obtained using a simple power function.

Furthermore, approximate linear relationships between $V_m/V_{m,0}$ or $L_m/L_{m,0}$ and α was established to get a more general, concise, and applicable scaling law. Then we compared the predicted values based on the new scaling law with those given by the previous relationship without considering the grain orientation, as well as the experimental data measured from in situ and real-time observation of Al-Cu alloys solidification by synchrotron X-ray radiography. Despite large discrepancy between the predicted values and the experimental data, most likely due to the different nucleation times of the interacted grains, the new scaling law proposed in the present work could still give predictions which are in much better agreement with the experimental results than the original scaling law for $\alpha = 0$. In the future work, other complex factors in the actual polycrystalline solidification will be considered, such as the nucleation time difference as just mentioned, the cooling rate, and the liquid natural convection arising from the uneven distribution of solute, and even the case where two grains are not mirror symmetric. Then a more general scaling law to be applied in complex solidification conditions is likely to be established. To further validate the scaling law

proposed in the present work, it would also be interesting to perform solidification experiments in which grain nucleations are simultaneously provoked in the sample.

Acknowledgement

This work was supported by the National Natural Science Foundation of China (No. 52203301), the China Postdoctoral Science Foundation (No. 2021TQ0335), the Young Talents Project of SYNL (No. 2021000559), and the Strategic Priority Research Program of the Chinese Academy of Sciences (No. XDC04000000). This work was also supported by the French National Space Agency (CNES), focused on MASER-14 sounding rocket mission.

References

[1]W. Kurz, D.J. Fisher, R. Trivedi Progress in modelling solidification microstructures in metals and alloys: dendrites and cells from 1700 to 2000 Int. Mater. Rev., 64 (2019), pp. 311-354

[2]W. Kurz, M. Rappaz, R. Trivedi Progress in modelling solidification microstructures in metals and alloys. Part II: dendrites from, to 2018 Int. Mater. Rev., 66 (2021) (2001), pp. 30-76

[3] A. Bogno, H. Nguyen-Thi, G. Reinhart, B. Billia, J. Baruchel Growth and interaction of dendritic equiaxed grains: In situ characterization by synchrotron X-ray radiography Acta Mater., 61 (2013), pp. 1303-1315

[4] M. Becker, S. Klein, F. Kargl Free dendritic tip growth velocities measured in Al-Ge Phys. Rev. Mater., 2 (2018), Article 073405

[5] A. Karma, W.J. Rappel Quantitative phase-field modeling of dendritic growth in two and three dimensions Phys. Rev. E, 57 (1998), pp. 4323-4349

[6] A. Karma Phase-field formulation for quantitative modeling of alloy solidification Phys. Rev. Lett., 87 (2001), Article 115701

[7] B. Echebarria, R. Folch, A. Karma, M. Plapp Quantitative phase-field model of alloy solidification Phys. Rev. E, 70 (2004), Article 061604

[8] W.J. Boettinger, J.A. Warren, C. Beckermann, A. Karma Phase-field simulation of solidification Annu. Rev. Mat. Res., 32 (2002), pp. 163-194

[9] T. Takaki Phase-field modeling and simulations of dendrite growth ISIJ Int., 54 (2014), pp. 437-444

[10] A. Karma, D. Tourret Atomistic to continuum modeling of solidification microstructures Curr. Opin. Solid State Mater. Sci., 20 (2016), pp. 25-36

[11] A. Yamanaka, T. Aoki, S. Ogawa, T. Takaki GPU-accelerated phase-field simulation of dendritic solidification in a binary alloy J. Cryst. Growth, 318 (2011), pp. 40-45

[12] T. Takaki, S. Sakane, M. Ohno, Y. Shibuta, T. Shimokawabe, T. Aoki Primary arm array during directional solidification of a single-crystal binary alloy: Large-scale phase-field study Acta Mater., 118 (2016), pp. 230-243

[13] C. Yang, Q.Y. Xu, B.C. Liu GPU-accelerated three-dimensional phase-field simulation of dendrite growth in a nickel-based superalloy Comput. Mater. Sci, 136 (2017), pp. 133-143

[14] T.Z. Gong, Y. Chen, Y.F. Cao, X.H. Kang, D.Z. Li Fast simulations of a large number of crystals growth in centimeter-scale during alloy solidification via nonlinearly preconditioned quantitative phase-field formula Comput. Mater. Sci, 147 (2018), pp. 338-352

[15] Y. Chen, D.Z. Li, B. Billia, H. Nguyen-Thi, X.B. Qi, N.M. Xiao Quantitative phase-field simulation of dendritic equiaxed growth and comparison with in situ observation on Al-4 wt.% Cu alloy by means of synchrotron X-ray radiography ISIJ Int., 54 (2014), pp. 445-451

[16] A.K. Boukellal, J.-M. Debierre, G. Reinhart, H. Nguyen-Thi Scaling laws governing the growth and interaction of equiaxed Al-Cu dendrites: A study combining experiments with phase-field simulations Materialia, 1 (2018), pp. 62-69

[17] A.K. Boukellal, M. Rouby, J.M. Debierre Tip dynamics for equiaxed Al-Cu dendrites in thin samples : Phase-field study of thermodynamic effects Comput. Mater. Sci, 186 (2021), Article 110051

[18] T.Z. Gong, Y. Chen, S.S. Li, Y.F. Cao, L.Y. Hou, D.Z. Li, X.Q. Chen, G. Reinhart, H. Nguyen Equiaxed dendritic growth in nearly isothermal conditions: A study combining in situ and real-time experiment with large-scale phase-field simulation Mater. Today Commun., 28 (2021), Article 102467

[19] Y. Chen, A.A. Bogno, N.M. Xiao, B. Billia, X.H. Kang, H. Nguyen-Thi, X.H. Luo, D.Z. Li Quantitatively comparing phase-field modeling with direct real time observation by synchrotron X-ray radiography of the initial transient during directional solidification of an Al-Cu alloy Acta Mater., 60 (2012), pp. 199-207

[20] Y. Chen, B. Billia, D.Z. Li, H. Nguyen-Thi, N.M. Xiao, A.A. Bogno Tip-splitting instability and transition to seaweed growth during alloy solidification in anisotropically preferred growth direction Acta Mater., 66 (2014), pp. 219-231

[21] A.J. Clarke, D. Tourret, Y. Song, S.D. Imhoff, P.J. Gibbs, J.W. Gibbs, K. Fezzaa, A. Karma Microstructure selection in thin-sample directional solidification of an Al-Cu alloy: In situ X-ray imaging and phase-field simulations Acta Mater., 129 (2017), pp. 203-216

[22] K. Glasner Nonlinear preconditioning for diffuse interfaces J. Comput. Phys., 174 (2001), pp. 695-711

[23] W. Bangerth, D. Davydov, T. Heister, L. Heltai, G. Kanschat, M. Kronbichler, M. Maier, B. Turcksin, D. Wells The deal.II library, version 8.4 J. Numer. Math., 24 (2016), pp. 135-141

[24] T.Z. Gong, A.K. Boukellal, Y. Chen, J.M. Debierre Equiaxed growth of interacting Al–Cu dendrites in thin samples: a phase-field study at copper concentrations relevant for practical applications Comptes Rendus Mécanique, 351 (2023), pp. 1-15